Role of Energy Distribution in Multicomponent Sorption Kinetics in Bidispersed Solids

Xijun Hu and Duong D. Do
Dept. of Chemical Engineering, University of Queensland, Brisbane, Queensland 4072, Australia

The heterogeneous macropore, surface and micropore diffusion model recently proposed by Hu et al. (1993) for single-component systems is extended to multicomponent systems in the description of sorption kinetics of gaseous adsorbates in bidispersed (macropore and micropore diffusions), heterogeneous microporous particles. This model describes sorption of gaseous adsorbates with allowance for the energy distribution of adsorption site for both equilibrium and diffusion of the adsorbed species. A uniform distribution is used to describe this energy distribution, and the cumulative energy distribution function is assumed the same for all species in the analysis of multicomponent mixtures. Extensive experimental data of ethane and propane in Ajax activated carbon are collected to study the effects of energy distribution on the binary adsorption, desorption, and displacement dynamics.

Introduction

The surface energetic heterogeneity concept has long been recognized in the measurement of adsorption equilibrium isotherms of gases (Roginski, 1948, 1958; Ross and Olivier, 1961; Misra, 1970; Sircar, 1984; Sircar and Myers, 1988). However, studies of the effect of this surface energetic heterogeneity on the surface diffusion are very limited (Okazaki et al., 1981; Zgrablich et al., 1986; Horas et al., 1988; Seidel and Carl, 1989; Kapoor and Yang, 1989, 1990). The role of surface energetic heterogeneity in the sorption dynamics is recently studied by Do and Hu (1993) and Hu et al. (1993) for single component systems. It is important to have a mathematical model to predict the multicomponent sorption dynamics from only information about single species because of the many possible combinations of parameters in multicomponent systems and because all industrial adsorption processes involve more than one adsorbate. Although the surface energetic heterogeneity has been widely investigated in the study of multicomponent equilibria (Myers, 1984; Valenzuela et al., 1988; Moon and Tien, 1988; Kapoor et al., 1990), it has rarely been considered in the multicomponent dynamics.

In the studies of Hu and Do (1993a), a heterogeneous macropore and surface diffusion (HMSD) model is proposed for large particles where the micropore resistance is negligible compared to the resistance along the particle coordinate. The diffusional resistance into the micropores becomes significant compared to the macropore resistance when the particles are made smaller. Therefore, it is necessary to include the micropore diffusion mechanism in the mathematical modeling to describe the sorption kinetics for all particle sizes. To reach this objective, a heterogeneous macropore, surface and micropore diffusion (HMSMD) model is proposed in this article. In this model, the heterogeneous diffusion of adsorbed species is allowed for in both particle and microparticle directions. The local diffusion flux of adsorbed species inside the microparticle is calculated with an aid of an imaginary gas phase concentration, a concept proposed earlier by Hu and Do (1993b). The local diffusion of adsorbed species is governed by a chemical potential gradient driving force on a single patch, and the overall flux is obtained by integration of the local flux over a distribution of adsorption sites. By taking into account the effects of surface energetic heterogeneity on both dynamics and equilibria, this model is more fundamental and provides better predictions than the corresponding MSMD model we recently proposed (Hu and Do, 1993b) on the multicomponent dynamic data, using only information of single component mass transfer and equilibria.

Theory

A heterogeneous microporous particle is exposed to a bulk environment containing NC adsorbate species. The assumptions in the model development are:

Correspondence concerning this article should be addressed to D. D. Do.

(1) The system is isothermal.

(2) The bulk is large enough so that the bulk concentrations are constant.

(3) Both free and adsorbed species diffuse inside the particle.

(4) The adsorbed species diffuse along the directions of both particle and microparticle coordinates.

(5) The particle surface is heterogeneous in the sense that there is a distribution of interaction energies between the adsorbate and adsorbent.

(6) The pore diffusivity, film mass-transfer coefficient and the surface diffusivity at zero surface loading are constant.

Local adsorption isotherm and energy distribution

The local adsorption isotherm for a given site with an adsorption energy $E(k)$ for the species k is assumed to follow the extended Langmuir equation of the following form:

$$C_\mu[k,E(k)] = C_{\mu s}(k)\,\frac{b[k,E(k)]C_p(k)}{1+\sum_{j=1}^{NC} b[j,E(j)]C_p(j)} \tag{1}$$

where C_p is the gas phase concentration, $C_{\mu s}$ is the maximum adsorbed phase concentration, $C_\mu[k,E(k)]$ and $b[k,E(k)]$ are the adsorbed phase concentration and the affinity for adsorbate k for a given site of energy $E(k)$, respectively, and the affinity is correlated to the interaction energy by the following equation:

$$b[k,E(k)] = b_0(k)\exp\left(\frac{E(k)}{RT}\right) \tag{2}$$

with b_0 being the affinity at the zero energy level or at the infinite temperature.

Let the energy distribution in the adsorbed phase be $F[k,E(k)]$, the macroscopically observed isotherm at a given set of gas phase concentration $C_p(k)$ $(k=1, NC)$ is:

$$C_{\mu\,\mathrm{obs}}(k) = C_{\mu s}(k)\int_0^\infty \frac{b[k,E(k)]C_p(k)}{1+\sum_{j=1}^{NC} b[j,E(j)]C_p(j)}\,F[k,E(k)]\,dE(k) \tag{3}$$

where the energy distribution function satisfies the following equation:

$$\int_0^\infty F[k,E(k)]dE(k) = 1 \tag{4}$$

In this article, we will only discuss the uniform energy distribution which has the following form:

$$F[k,E(k)] = \frac{1}{E_{\max}(k)-E_{\min}(k)} \quad \text{for } E_{\min}(k) < E < E_{\max}(k) \tag{5}$$

and $F[k,E(k)]=0$ elsewhere. By assuming that the ordering of the energy sites from low to high is the same for different adsorbates and the cumulative energy distribution function is the same for all species in the mixture (Valenzuela et al., 1988), the correlation of energies of different species for a uniform energy distribution is (Kapoor et al., 1990):

$$\frac{E(i)-E_{\min}(i)}{E_{\max}(i)-E_{\min}(i)} = \frac{E(j)-E_{\min}(j)}{E_{\max}(j)-E_{\min}(j)} \tag{6}$$

where the whole energy distribution region of one species is matched to that of another species.

The extended Langmuir equation has been used for the local adsorption isotherm (Eq. 1), hence, it is required for different species to have the same maximum adsorption capacities in order to be thermodynamically consistent.

Local diffusion flux of the adsorbed species

If the adsorbed species is in local equilibrium with the free species, by using the chemical potential gradient as the driving force for the diffusion of the adsorbed species, the diffusion flux of the adsorbed species k at the energy level $E(k)$ can be written as (Hu and Do, 1993a):

$$J_\mu[k,E(k)] = -D_\mu[k,E(k)]\,\frac{C_\mu[k,E(k)]}{C_p(k)}\,\frac{\partial C_p(k)}{\partial r} \tag{7}$$

or in terms of the adsorbed concentration gradients:

$$J_\mu[k,E(k)] = -D_\mu[k,E(k)]\,\frac{C_\mu[k,E(k)]}{C_p(k)}\sum_{j=1}^{NC}\frac{\partial C_p(k)}{\partial C_\mu[j,E(j)]}\,\frac{\partial C_\mu[j,E(j)]}{\partial r} \tag{8}$$

with $D_\mu[k,E(k)]$ having the following functional dependence on temperature:

$$D_\mu[k,E(k)] = D_{\mu 0}(k)\exp\left(-\frac{a(k)E(k)}{R_g T}\right) \tag{9}$$

and $D_{\mu 0}(k)$ being the surface diffusivity of zero energy at zero loading of species k.

If the adsorbed species are in local equilibrium with the free species, its diffusion flux can be described by Eq. 7 or 8. Unfortunately, this is not the case in medium or small sized particles as due to the micropore resistance inside the microparticle, there is a distribution of adsorbed concentration along the micropore coordinate. This means that with the exception of the adsorbed species at the microparticle exterior surface, the interior adsorbed species are not in local equilibrium with the concentration of the free species. To describe the diffusion flux of the adsorbed species *inside* the microparticle, the imaginary gas phase concentration concept proposed earlier by Hu and Do (1993b) is adopted. Let the set of free species having imaginary concentrations, $C_{im}(k)$ $(k=1$ to NC) be in equilibrium with the adsorbed species inside the microparticle having concentrations $C_\mu(k)$ $(k=1$ to NC). These imaginary gas concentrations are calculated from the multicomponent equilibrium equations from the adsorbed phase concentrations for any point inside the microparticle. The distribution of the adsorbed phase concentration inside the microparticle is governed by the differential mass balance equation in the microparticle (Eq. 13). At the exterior surface of the microparticle,

these imaginary concentrations are equal to the macropore concentrations ($C_p(k)$) as the adsorbed concentrations at the exterior surface are in equilibrium with $C_p(k)$:

$$r_\mu = R_\mu; \quad C_{im}(k) = C_p(k) \text{ for } k = 1, 2, \ldots, \text{NC}. \tag{10}$$

We denote the coordinate along the particle as r with a diffusion length of R. This is the direction that the free and adsorbed species penetrates into the particle (particle direction). The coordinate in the grain is defined as r_μ with a diffusion length of R_μ (length scale of the micropore diffusional resistance); this is the direction that the adsorbed species have to diffuse into its own domain of microparticle (microparticle direction, Hu and Do, 1993b). The zero coverage surface diffusivity with zero energy, $D_{\mu 0}$, is assumed to be different in the grain coordinate from that in the particle coordinate by a factor of β^2, that is, $D_{\mu 0}(r_\mu) = \beta^2 D_{\mu 0}(r)$. The reason for this is that different species with different molecular sizes can access the micropores with different degrees because of the micropore distributions; hence, the tortuosity in the micropores can be different for different components, as stated in Hu and Do (1993b) and Hu et al. (1993). By using the imaginary concentration concept, we can write the fluxes of the adsorbed species at the energy level E along the corresponding two coordinates as follows:

$$J_\mu[k,E(k)]_r = -D_\mu[k,E(k)] \frac{C_\mu[k,E(k)]}{C_{im}(k)} \frac{\partial C_{im}(k)}{\partial r} \tag{11}$$

$$J_\mu[k,E(k)]_{r_\mu} = -\beta^2 D_\mu[k,E(k)] \frac{C_\mu[k,E(k)]}{C_{im}(k)} \frac{\partial C_{im}(k)}{\partial r_\mu} \tag{12}$$

with $D_\mu[k,E(k)]$ following the correlation of Eq. 9.

Mass balance equations

Having obtained the expression of the diffusion flux of the adsorbed species, the mass balance equation in the microparticle can be written as:

$$\frac{\partial}{\partial t} \int_0^\infty C_\mu[k,E(k)]F[k,E(k)]dE(k) = -\frac{1}{r_\mu^{s_\mu}} \frac{\partial}{\partial r_\mu} \left(r_\mu^{s_\mu} \int_0^\infty J_\mu[k,E(k)]_{r_\mu} F[k,E(k)]dE(k) \right) \tag{13}$$

where s_μ is the geometric factor of the microparticle (=0, 1 and 2 for slab, cylinder and sphere, respectively), $F[k,E(k)]$ is the energy distribution of species k, and the flux $J_\mu[k,E(k)]_{r_\mu}$ is given in Eq. 12.

The local adsorbed concentrations inside the microparticle are written in terms of the imaginary gas phase concentration, as explained in Eq. 10:

$$C_\mu[k,E(k)] = C_{\mu s}(k) \frac{b[k,E(k)]C_{im}(k)}{1 + \sum_{j=1}^{\text{NC}} b[j,E(j)]C_{im}(j)} \tag{14}$$

The corresponding boundary conditions of Eq. 13 are:

$$r_\mu = 0; \quad \frac{\partial C_\mu[k,E(k)]}{\partial r_\mu} = 0 \tag{15}$$

$$r_\mu = R_\mu; \quad \int_0^\infty C_\mu[k,E(k)]F[k,E(k)]dE(k) = \int_0^\infty C_{\mu s}(k) \frac{b[k,E(k)]C_p(k)}{1 + \sum_{j=1}^{\text{NC}} b[j,E(j)]C_p(j)} F[k,E(k)]dE(k) \tag{16}$$

The total mass balance equation for the particle is:

$$\epsilon_M \frac{\partial C_p(k)}{\partial t} + (1-\epsilon_M) \frac{\int_0^{R_\mu} \frac{\partial}{\partial t} \left(\int_0^\infty C_\mu[k,E(k)]F[k,E(k)]dE(k) \right) r_\mu^{s_\mu} dr_\mu}{\int_0^{R_\mu} r_\mu^{s_\mu} dr_\mu} = -\epsilon_M \frac{1}{r^s} \frac{\partial}{\partial r} [r^s J_p(k)] - (1-\epsilon_M) \frac{1}{r^s} \frac{\partial}{\partial r} \times \left[r^s \frac{\int_0^{R_\mu} \left(\int_0^\infty J_\mu[k,E(k)]_r F[k,E(k)]dE(k) \right) r_\mu^{s_\mu} dr_\mu}{\int_0^{R_\mu} r_\mu^{s_\mu} dr_\mu} \right] \tag{17}$$

where s is the particle shape factor, with a value 0, 1 or 2 being for slab, cylinder or sphere, respectively, ϵ_M is the macropore porosity, and J_p is the pore diffusion flux. The local adsorbed concentration inside the microparticle is calculated from Eq. 14.

In Eqs. 13 and 17, the parallel-path model (PPM) by Kapoor and Yang (1989) has been adopted to describe the diffusion of adsorbed species. By assuming that the adsorbed phase consists of a series of parallel paths such that each path has a uniform but different energy, and the adsorbed species diffuse in the direction of these parallel paths, the PPM has a comparable accuracy with a two-dimensional effective medium approximation (Kapoor and Yang, 1990) where the diffusion of molecules from one patch of energy to another patch of different energy is allowed.

The first term in the LHS and RHS of Eq. 17 are self-explainable. The second term in the LHS and RHS are the average accumulation and the average mass transfer along the particle coordinate contributed by the surface diffusion of the adsorbed species, respectively.

The boundary conditions of the mass balance equation in the macropore are:

$$r = 0; \quad \frac{\partial C_p(k)}{\partial r} = 0 \tag{18}$$

$$r=R;\ \epsilon_M J_p(k)+(1-\epsilon_M)\times\frac{\int_0^{R_\mu}\left(\int_0^\infty J_\mu[k,E(k)],F[k,E(k)]dE(k)\right)r_\mu^{s_\mu}dr_\mu}{\int_0^{R_\mu}r_\mu^{s_\mu}dr_\mu}=k_m(k)[C_p(k)-C_b(k)] \quad (19)$$

The initial conditions of the model equations are:

$$t=0;\quad C_p(k)=C_{pi}(k);\quad C_\mu[k,E(k)]=C_{\mu s}(k)\frac{b[k,E(k)]C_{pi}(k)}{1+\sum_{j=1}^{NC}b[j,E(j)]C_{pi}(j)} \quad (20)$$

Nondimensional model equations

By defining the nondimensional variables and parameters as shown in Table 1, the HMSMD model equations are cast into nondimensional form to facilitate numerical calculations. The resulting nondimensional mass balance equation in the microparticle is

$$\sigma_\mu(k)\frac{\partial}{\partial\tau}\int_0^\infty Y_\mu[k,e(k)]f[k,e(k)]de(k)=\gamma(k)\frac{1}{x_\mu^{s_\mu}}\times\frac{\partial}{\partial x_\mu}\left(x_\mu^{s_\mu}\int_0^\infty H[k,e(k)]\frac{Y_\mu[k,e(k)]}{Y_{im}(k)}\frac{\partial Y_{im}(k)}{\partial x_\mu}f[k,e(k)]de(k)\right) \quad (21)$$

with the corresponding boundary conditions in nondimensional form being

$$x_\mu=0;\quad \frac{\partial Y_\mu[k,e(k)]}{\partial x_\mu}=0 \quad (22)$$

$$x_\mu=1;\quad \int_0^\infty Y_\mu[k,e(k)]f[k,e(k)]de(k)=\frac{C_{\mu s}(k)}{C_{\mu 0}(k)}\int_0^\infty\left[\frac{\lambda[k,e(k)]Y(k)}{1+\sum_{j=1}^{NC}\lambda[j,e(j)]Y(j)}\right]_x f[k,e(k)]de(k) \quad (23)$$

The nondimensional mass balance equation in the particle is:

$$\sigma(k)\frac{\partial Y(k)}{\partial\tau}+\sigma_\mu(k)\frac{\int_0^1\left(\frac{\partial}{\partial\tau}\int_0^\infty Y_\mu[k,e(k)]f[k,e(k)]de(k)\right)x_\mu^{s_\mu}dx_\mu}{\int_0^1 x_\mu^{s_\mu}dx_\mu}=\eta(k)\frac{1}{\partial x^s}\frac{\partial}{\partial x}\left(x^s\frac{\partial Y(k)}{\partial x}\right)+\delta(k)\frac{1}{x^s}\frac{\partial}{\partial x}\left\{x^s\frac{\int_0^1\left(\int_0^\infty H[k,e(k)]\frac{Y_\mu[k,e(k)]}{Y_{im}(k)}\frac{\partial Y_{im}(k)}{\partial x}f[k,e(k)]de(k)\right)x_\mu^{s_\mu}dx_\mu}{\int_0^1 x_\mu^{s_\mu}dx_\mu}\right\} \quad (24)$$

with nondimensional boundary conditions being

$$x=0;\quad \frac{\partial Y(k)}{\partial x}=0 \quad (25)$$

$$x=1;\quad \eta(k)\frac{\partial Y(k)}{\partial x}+\delta(k)\frac{\int_0^1\left(\int_0^\infty H[k,e(k)]\frac{Y_\mu[k,e(k)]}{Y_{im}(k)}\frac{\partial Y_{im}(k)}{\partial x}f[k,e(k)]de(k)\right)x_\mu^{s_\mu}dx_\mu}{\int_0^1 x_\mu^{s_\mu}dx_\mu}=Bi[Y_b(k)-Y(k)] \quad (26)$$

Solution Methods

A Gaussian (RADAU) quadrature (Villadsen and Michelsen, 1978) is used to evaluate the integrals involving the energy distribution:

$$\int_0^\infty J_\mu[k,E(k)]F[k,E(k)]dE(k)=\int_0^1 J_\mu[k,x_e(k)]g[k,x_e(k)]dx_e(k)=\sum_{ie=1}^{NT}J_\mu[k,x_e(k,ie)]g[k,x_e(k,ie)]we(ie) \quad (27)$$

$$\int_0^\infty C_\mu[k,E(k)]F[k,E(k)]dE(k)=\int_0^1 C_\mu[x_e(k)]g[x_e(k)]dx_e(k)=\sum_{ie=1}^{NT}C_\mu[x_e(k,ie)]g[x_e(k,ei)]we(ie) \quad (28)$$

where x_e is a variable used to normalize the integral range and $we(ie)$ is the quadrature weight at each node point $x_e(k,ie)$. In particular, for a uniform energy distribution, we have:

$$F[k,E(k)]=\frac{1}{E_{\max}(k)-E_{\min}(k)}\quad \text{for } E_{\min}(k)<E(k)<E_{\max}(k) \quad (29)$$

Table 1. Definition of Nondimensional Variables and Parameters

$$e(k)=\frac{E(k)}{R_gT};\quad f[k,\,e(k)]=F[k,\,E(k)]R_gT;$$

$$\bar{e}(k)=\int_0^\infty e(k)f[k,\,e(k)]de(k)$$

$$\lambda[k,\,e(k)]=b_0(k)\exp(e(k))C_0(k);\quad H[k,\,e(k)]=\exp[a(k)(\bar{e}(k)-e(k))]$$

$$Y(k)=\frac{C_p(k)}{C_0(k)};\quad Y_b(k)=\frac{C_b(k)}{C_0(k)};\quad Y_{im}(k)=\frac{C_{im}(k)}{C_0(k)}$$

$$Y_\mu[k,\,e(k)]=\frac{C_\mu[k,\,E(k)]}{C_{\mu0}(k)};$$

$$C_{\mu0}(k)=C_{\mu s}(k)\int_0^\infty\frac{\lambda[k,\,e(k)]}{1+\sum_{j=1}^{NC}\lambda[j,\,e(j)]}f[k,\,e(k)]de(k)$$

$$x=\frac{r}{R};\quad x_\mu=\frac{r_\mu}{R_\mu}$$

$$\tau=\frac{\left(\epsilon_M\sum_{k=1}^{NC}D_p(k)C_0(k)+(1-\epsilon_M)\sum_{k=1}^{NC}D_{\mu0}(k)e^{-a(k)\bar{e}(k)}C_{\mu0}(k)\right)t}{R^2\left[\epsilon_M\sum_{k=1}^{NC}C_0(k)+(1-\epsilon_M)\sum_{k=1}^{NC}C_{\mu0}(k)\right]}$$

$$\sigma(k)=\frac{\epsilon_MC_0(k)}{\epsilon_M\sum_{j=1}^{NC}C_0(j)+(1-\epsilon_M)\sum_{j=1}^{NC}C_{\mu0}(j)}$$

$$\sigma_\mu(k)=\frac{(1-\epsilon_M)C_{\mu0}(k)}{\epsilon_M\sum_{j=1}^{NC}C_0(j)+(1-\epsilon_M)\sum_{j=1}^{NC}C_{\mu0}(j)}$$

$$\eta(k)=\frac{\epsilon_MD_p(k)C_0(k)}{\epsilon_M\sum_{j=1}^{NC}D_p(j)C_0(j)+(1-\epsilon_M)\sum_{j=1}^{NC}D_{\mu0}(j)e^{-a(j)\bar{e}(j)}C_{\mu0}(j)}$$

$$\delta(k)=\frac{(1-\epsilon_m)D_{\mu0}(k)e^{-a(k)\bar{e}(k)}C_{\mu0}(k)}{\epsilon_M\sum_{j=1}^{NC}D_p(j)C_0(j)+(1-\epsilon_M)\sum_{j=1}^{NC}D_{\mu0}(j)e^{-a(j)\bar{e}(j)}C_{\mu0}(j)}$$

$$Bi(k)=\frac{k_m(k)RC_0(k)}{\epsilon_M\sum_{j=1}^{NC}D_p(j)C_0(j)+(1-\epsilon_M)\sum_{j=1}^{NC}D_{\mu0}(j)e^{-a(j)\bar{e}(j)}C_{\mu0}(j)}$$

$$\gamma(k)=\delta(k)\left(\frac{\beta(k)R}{R_\mu}\right)^2$$

and $F[k,E(k)]=0$ elsewhere. Hence,

$$x_e(k)=\frac{E(k)-E_{\min}(k)}{E_{\max}(k)-E_{\min}(k)};\quad g[k,x_e(k)]=1 \tag{30}$$

and

$$E(k)=E_{\min}(k)+x_e(k)[E_{\max}(k)-E_{\min}(k)] \tag{31}$$

The average accumulation of the adsorbed species within the microparticle

$$\frac{\int_0^1\left(\frac{\partial}{\partial\tau}\int_0^\infty Y_\mu[k,e(k)]f[k,e(k)]de(k)\right)x_\mu^{s_\mu}dx_\mu}{\int_0^1x_\mu^{s_\mu}dx_\mu} \tag{32}$$

is also integrated by using the RADAU quadrature. The average diffusion flux of the adsorbed species along the particle coordinate is solved by a similar technique.

The nondimensional mass balance equations (Eqs. 21-26) are numerically solved by using the orthogonal collocation technique of Villadsen and Michelsen (1978) to transform the coupled partial differential equations to a larger set of coupled ordinary differential equations, which are effectively solved by the differential-algebraic equation solver (Petzold, 1982).

Experiments

Slab or cylinder particles of Ajax activated carbon were used as adsorbents. About 0.3 g of slabs or 0.2 g of cylinders was used in the dynamic studies. The experimental operation procedure of binary adsorption, desorption and displacement dynamics was similar to that of single-component systems described in Hu et al. (1993). The differences are highlighted below.

(1) Simultaneous adsorption: Ethane, propane and nitrogen were thoroughly mixed before the mixture was passed through the adsorber.

(2) Simultaneous desorption: The mixed ethane and propane in nitrogen were flushed through the adsorber for a sufficiently long time to reach equilibrium. This time scale information can be obtained from simultaneous adsorption experiments. Pure nitrogen was then flushed through the adsorber for a specified desorption time. The remaining adsorbates in the particle were then desorbed to the sample bomb for subsequent concentration analysis by GC.

(3) Displacement: One adsorbate was first adsorbed for a long enough time to reach equilibrium. Another adsorbate was then introduced to the adsorber for a predetermined time to displace the first species. The adsorbed amount of the second species and the remaining amount of the first species were desorbed to the sample bomb for analysis using the same technique for adsorption measurement.

(4) The total flow rate of all species passing through the adsorber was 500 cm^3/min for all experiments of simultaneous adsorption, desorption and displacement.

(5) The temperature used to desorb the species from the adsorber to the sample bomb is 150°C.

(6) The GC detector responses of both ethane and propane were calibrated once daily.

Results and Discussions

The analyses of adsorption equilibria and dynamics of ethane

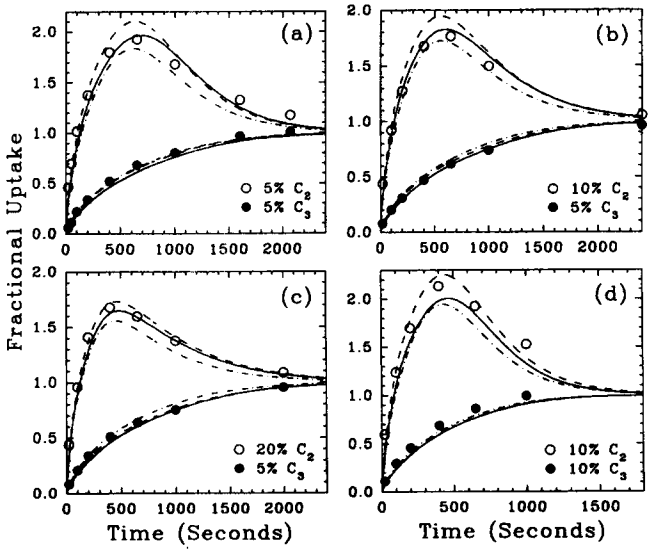

Figure 1. Binary adsorption dynamics of ethane and propane in Ajax activated carbon of 4.4 mm full length slabs at 10°C, 1 atm.

(——) HMSMD; (- - - -) MSMD; (-•-•-•-) CMSMD.

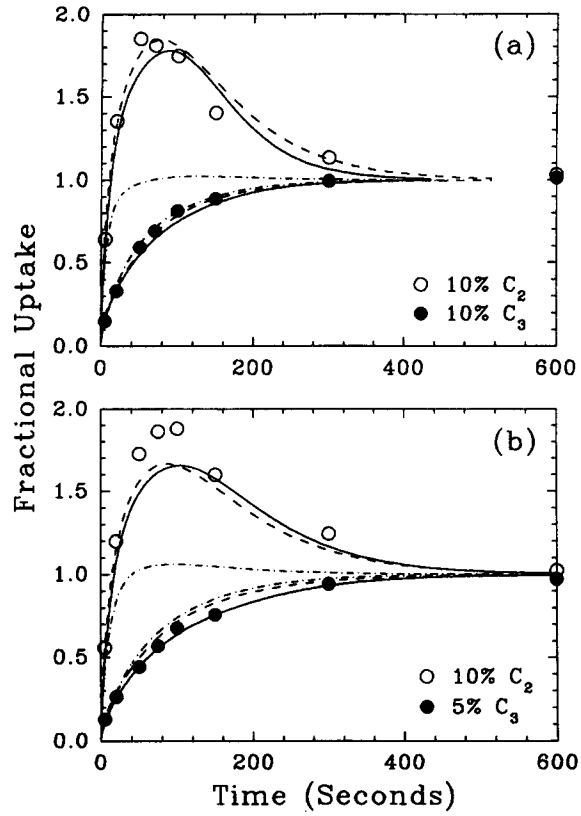

Figure 2. Binary adsorption dynamics of ethane and propane in Ajax activated carbon of 1/16 in. (1.6 mm) diameter cylinders at 10°C, 1 atm.

(——) HMSMD; (- - - -) MSMD; (-•-•-•-) CMSMD.

and propane in Ajax activated carbon for single-component systems have been carried out in Hu et al. (1993). In this section, we will use the isotherm and dynamic parameters of a single component obtained by Hu et al. (1993) and the multicomponent model presented in this article to *predict* the binary adsorption, desorption and displacement kinetics of ethane and propane in Ajax activated carbon under various conditions. The effects of the concentration dependent surface diffusion and the surface energetic heterogeneity on the binary adsorption, desorption and displacement kinetics of ethane and propane in Ajax activated carbon are studied by comparing the predictions of the HMSMD (this work), MSMD (Hu and Do, 1993b) and CMSMD (Gray and Do, 1990; Mayfield and Do, 1991) models along with the experimental data.

Simultaneous adsorption

Figure 1 shows the binary adsorption dynamics of ethane and propane under different concentration combinations onto Ajax activated carbon of 4.4 mm full length slabs at 10°C and 1 atm. For a 4.4 mm slab, the intraparticle mass-transfer process is dominated by the macropore resistance (Hu, 1992), of which 18% is contributed by the surface diffusional resistance. Since the mass transfer is mainly controlled by the pore diffusion, all three models are in good agreements with the experimental data, with the MSMD model slightly overpredicting the overshoot degree of ethane uptake and the CMSMD model underpredicting it. The difference between the HMSMD and MSMD predictions is narrowed with an increase in the ethane concentration (Figures 1a, 1b and 1c) or a decrease in the propane concentration (Figures 1b and 1d). This is physically expected because propane is more affected by the surface energetic heterogeneity (Hu et al., 1993).

The binary adsorption kinetics of ethane (10%) and propane (10 and 5%) onto 1/16 in. (1.6 mm) diameter cylinders of Ajax carbon is shown in Figure 2. The predictions from the CMSMD model are very poor. Little overshoot of the ethane uptake is observed for this model. Because the micropore resistance is significant in 1/16 in (1.6 mm) cylinder particles, the diffusion of the adsorbed species plays an important role in the intraparticle mass-transfer process. The predictions from the HMSMD and MSMD models are close to each other. This might be explained as below. In simultaneous adsorption, only ethane partly desorbs due to the displacement caused by the penetration of propane, while the uptake of propane behaves like that of a single-component system because of its higher affinity than that of ethane. In neither case, the role of energy distribution is significant as it has been shown in Hu et al. (1993) that this role is only significant in the desorption mode of propane.

The adsorption data collected at 30°C are used to further test the models. Plotted in Figure 3 are the binary adsorption dynamics of different concentrations of ethane (5 and 10%) together with 10% propane in Ajax carbon. Again the agreement between the CMSMD model predictions and the experimental data is found very poor for 1/16 in. (1.6 mm) cylindrical particles (Figures 3c and 3d). For a low ethane concentration (5%), the MSMD overpredicts the overshoot degree of ethane uptake in a 4.4 mm slab (Figure 3a). This overprediction is even more significant when the propane concentration is high (20%, Figure 4a). With this high propane concentration (20%), the fractional uptake of ethane (5%) is affected for a 1/16 in. (1.6 mm) cylinder. As seen in Figure 4b, the MSMD model

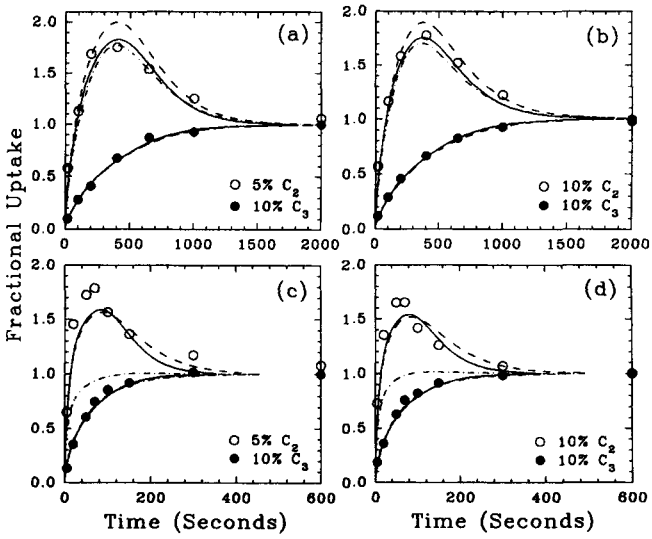

Figure 3. Binary adsorption dynamics of ethane and propane in Ajax activated carbon at 30°C, 1 atm.

(a), (b) 4.4 mm full length slab; (c), (d) 1/16 in. (1.6 mm) diameter cylinder. (——) HMSMD; (- - - -) MSMD; (-•-•-•-) CMSMD.

gives a long tail of the ethane uptake, while the HMSMD model provides a better prediction. In summary, the role of surface energetic heterogeneity is important when the ethane concentration is low and the propane concentration is high; otherwise,

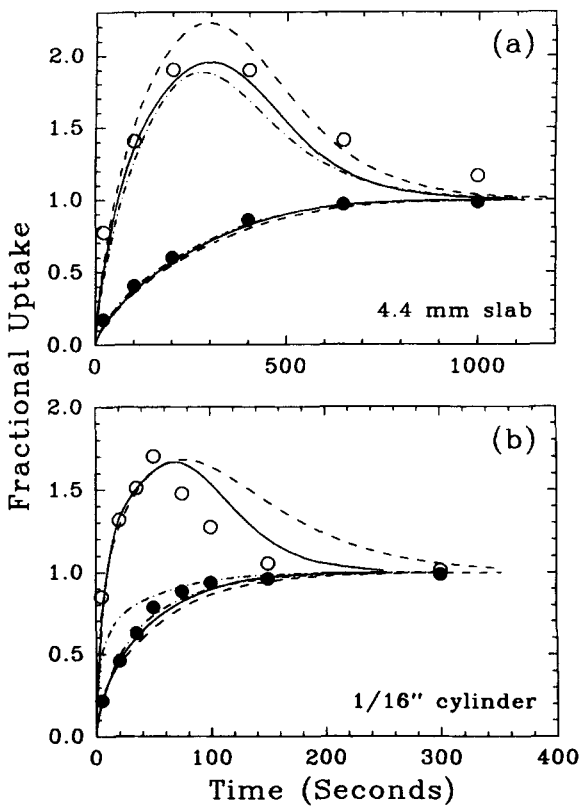

Figure 4. Binary adsorption dynamics of 5% ethane and 20% propane in Ajax activated carbon at 30°C, 1 atm.

(——) HMSMD; (- - - -) MSMD; (-•-•-•-) CMSMD.

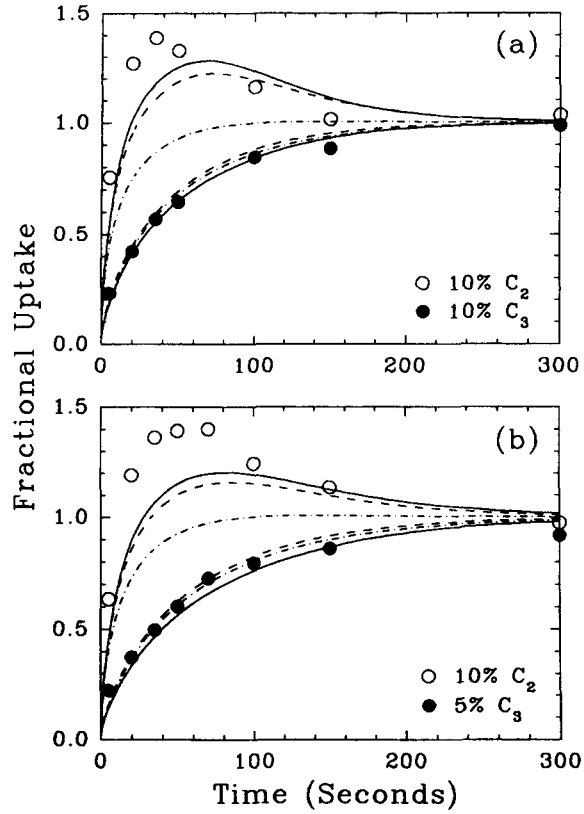

Figure 5. Binary adsorption dynamics of ethane and propane in Ajax activated carbon of 1/16 in. (1.6 mm) diameter cylinders at 60°C, 1 atm.

(——) HMSMD; (- - - -) MSMD; (-•-•-•-) CMSMD.

this effect is negligible in the simultaneous adsorption of ethane and propane.

For a higher temperature (60°C), although the HMSMD model provides a slightly better prediction for 1/16 in. (1.6 mm) cylindrical particles (Figure 5), it is nearly superimposed to the MSMD model for 4.4 mm slabs (Figure 6). The reason that the kinetics at 60°C is not sensitive to the surface energetic heterogeneity is that the energy distribution effect becomes less important in the adsorption equilibria as temperature increases (Hu et al., 1993). However, the CMSMD model still significantly underpredicts the overshoot degree of ethane uptake (Figure 5).

Simultaneous desorption

Up to now we have seen that the contribution of concentration dependent surface diffusion is very vital in the simultaneous adsorption of ethane and propane in Ajax activated carbon. The energy distribution also plays an important role in the binary adsorption dynamics when it is so in the description of equilibrium isotherm data. In this section, these two effects will be further investigated for the simultaneous desorption kinetics of ethane and propane in Ajax activated carbon.

The simultaneous desorption of 10% ethane and 10% propane at 30°C in Ajax activated carbon of different particle sizes and shapes, 4.4 and 2.6 mm full length slabs and 1/16 in. (1.6 mm)

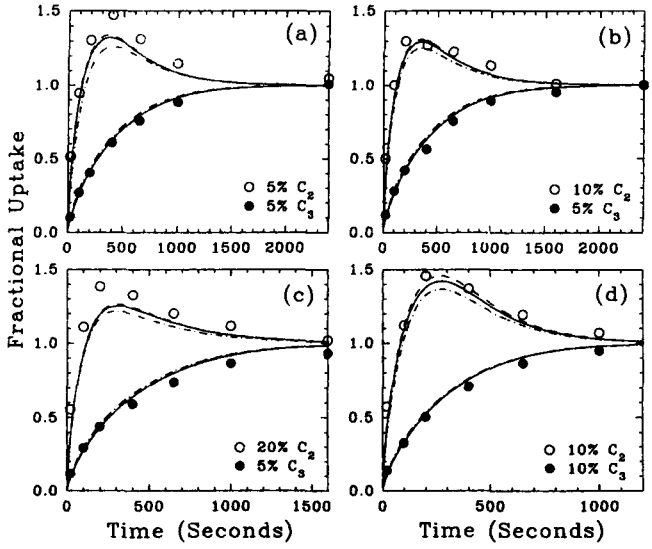

Figure 6. Binary adsorption dynamics of ethane and propane in Ajax activated carbon of 4.4 mm full length slabs at 60°C, 1 atm.

(——) HMSMD; (- - - -) MSMD; (-•-•-•-) CMSMD.

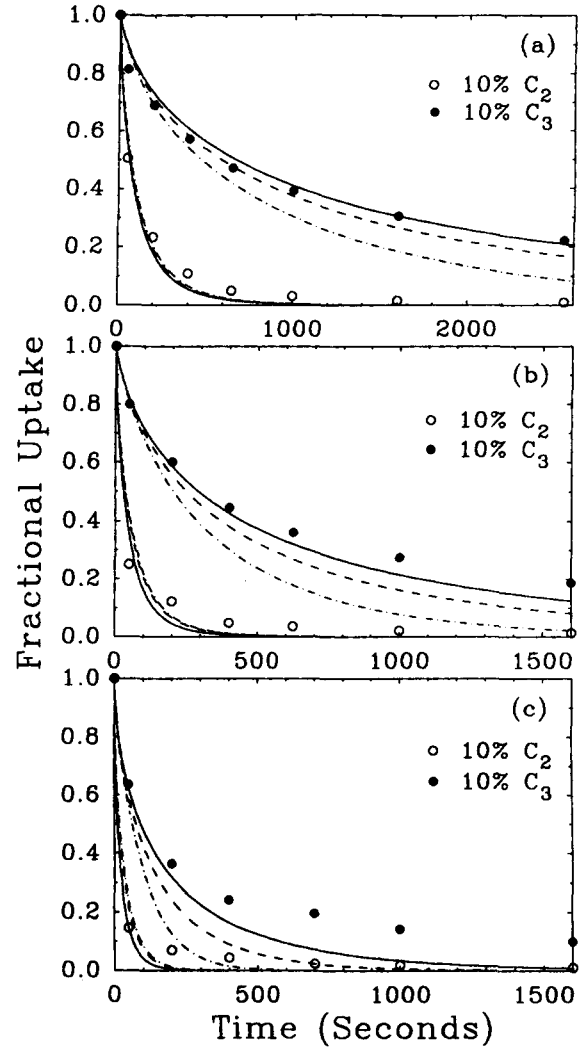

Figure 7. Binary desorption dynamics of ethane and propane in Ajax activated carbon at 30°C, 1 atm.

(a) 4.4 mm slab; (b) 2.6 mm slab, (c) 1/16 in. (1.6 mm) cylinder.
(——) HMSMD; (- - - -) MSMD; (-•-•-•-) CMSMD.

diameter cylinder, are shown in Figure 7. For slab particles (4.4 and 2.6 mm), the HMSMD model predictions are in good agreement with the experimental data; the MSMD model is not as good as the HMSMD model but can still describe the data reasonably well, while the CMSMD model is in serious error. For cylindrical particles, the HMSMD model best represents the data, followed by the MSMD model with the CMSMD model worst. The deviation of the HMSMD model from the experimental data in 1/16 in. (1.6 mm) cylinders might be due to the nonisothermal effect (some small temperature drops of less than 6°C are observed in the initial stage of desorption). It is reminded that the uptake process of ethane rather than that of propane is affected by the concentration dependent surface diffusion and the energy distribution in the simultaneous adsorption mode. However, significant differences between the three models are seen for the desorption of propane rather than that of ethane in the simultaneous desorption mode. This can be explained as below. In the single-component studies (Hu et al., 1993), we have found that all three models fit the adsorption kinetic data equally well; they differ only in the predictions of desorption dynamics, especially for propane due to its higher affinity. Now only ethane partly desorbs due to the interior displacement in the simultaneous adsorption mode, while both ethane and propane desorb in the simultaneous desorption mode. Therefore, the adsorption rate of ethane rather than propane is more affected by the choice of models in the simultaneous adsorption mode, while the desorption rate of propane is more significantly affected in the simultaneous desorption.

Figure 8 reveals the simultaneous desorption of ethane and propane in Ajax carbon of 1/16 in. (1.6 mm) diameter cylinders at 30°C with different concentration combinations, 10% ethane and 5% propane (Figure 8a) as well as 5% ethane and 10% propane (Figure 8b). The same conclusion as described in Figure 7 for cylindrical particles can be made here. In the prediction of propane desorption, the contribution of concentration dependent surface diffusion is more pronounced with an increase in propane concentration (see MSMD and CMSMD models in Figures 8a and 7c); while the effect of energy distribution is more significant at a lower propane concentration (see HMSMD and MSMD models in Figures 8a and 7c). The sorption rate of ethane is less affected by the choice of models at a higher ethane concentration (Figures 8b and 7c), which is also the case in the simultaneous adsorption.

The comparisons of the three models along with the experimental data are further carried out at another temperature, 10°C, as shown in Figure 9. The differences between the three models are larger here because the diffusion of adsorbed species contributes more to the total flux at 10°C because of the higher adsorption amount (Hu et al., 1993). Another reason is that the energy distribution is more important in the description of equilibrium isotherm data at 10°C (Hu et al., 1993). Again the HMSMD model is in very good agreement with the experimental data for 2.6 mm slab particles and some deviation exists for 1/16 in. (1.6 mm) cylindrical particles.

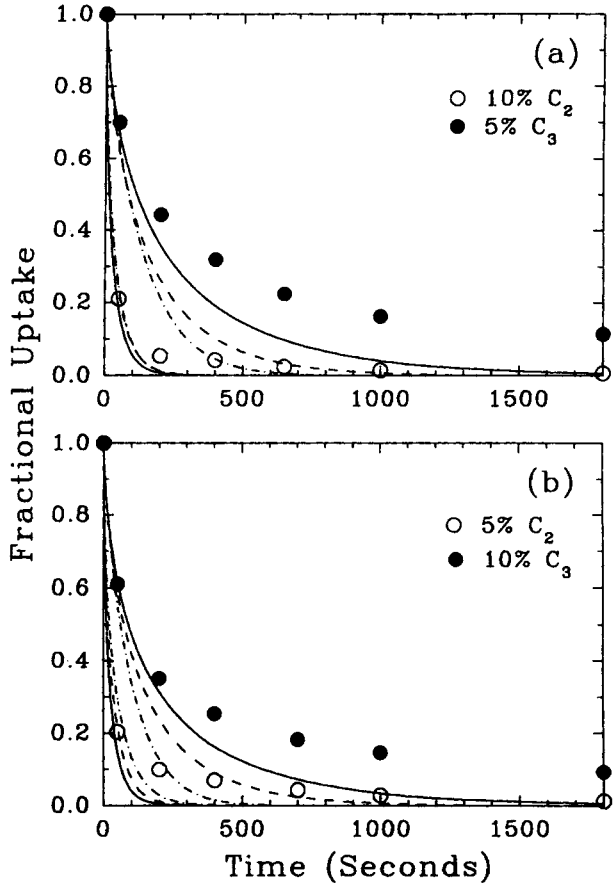

Figure 8. Binary desorption dynamics of ethane and propane in Ajax activated carbon of 1/16 in. diameter cylinders at 30°C, 1 atm.

(——) HMSMD; (- - - -) MSMD; (-•-•-•-) CMSMD.

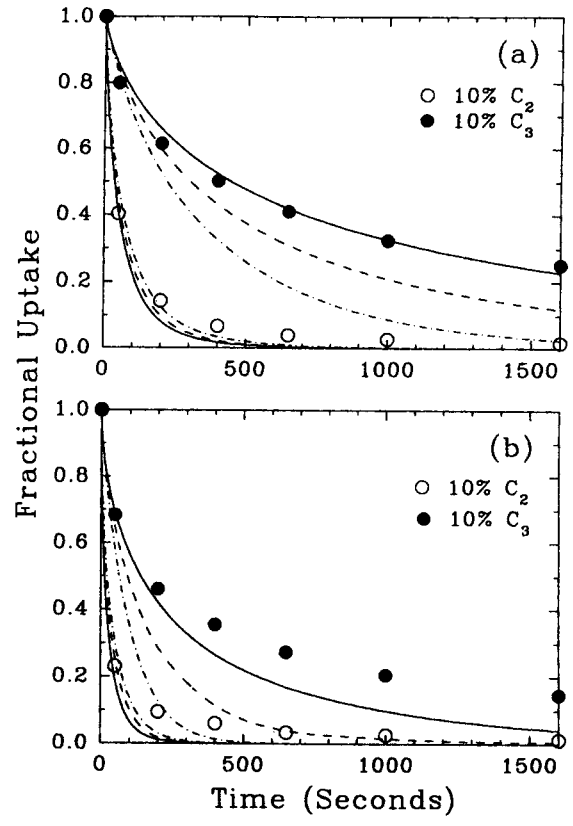

Figure 9. Binary desorption dynamics of 10% ethane and 10% propane in Ajax activated carbon at 10°C, 1 atm.

(a) 2.6 mm slab; (b) 1/16 in. (1.6 mm) cylinder. (——) HMSMD; (- - - -) MSMD; (-•-•-•-) CMSMD.

The above mentioned temperature effect is further confirmed by the simultaneous desorption dynamics at 60°C (Figure 10) where the differences between the three models are even narrowed. Unlike the cases in 10 and 30°C, the HMSMD model differs from the experimental data at 60°C even for the particle size of 2.6 mm full length. This is so because the desorption at 60°C is fast, the desorption rate for 2.6 mm slab is similar to that for 1/16 in. (1.6 mm) cylinder at 10°C (Figures 10a and 9b); hence deviation could be due to some nonisothermal effect.

In all binary desorption dynamic studies, it is seen that both effects of concentration dependent surface diffusion and energy distribution are significant in the predictions of propane desorption, although the desorption of ethane is less affected. These two effects become more important when the particle is smaller because of the greater contribution of the micropore resistance (diffusion of adsorbed species).

Displacement

Having analyzed the simultaneous adsorption and desorption kinetics, we now turn to the studies of effects of concentration dependent surface diffusion and energy distribution on displacement dynamics. Figure 11 shows the predictions of the three models (HMSMD, MSMD, and CMSMD) and the experimental data of the displacement dynamics of 10% ethane and 10% propane in Ajax activated carbon of 2.6 mm full length slabs at 30°C, either ethane displaced by propane (Figure 11a) or propane displaced by ethane (Figure 11b). It is observed that the HMSMD and MSMD models are close to each other and are in good agreement with the experimental data. The CMSMD model, on the other hand, although in the displacement of *ethane by propane* reasonably predicts propane adsorption with some deviation for ethane desorption, it is in serious error for uptakes of both ethane and propane in the displacement of *propane by ethane* where the desorbed species is propane.

The model comparisons are further carried out for another particle size and shape, 1/16 in. (1.6 mm) diameter cylinder, at 30°C for different concentration combinations, 10% ethane displaced by 10% propane (Figure 12a) and 10% ethane displaced by 5% propane (Figure 12b). Since the desorbed species here is ethane, all three models predict the displacement dynamics well while the CMSMD model slightly overpredicts the desorption rate of ethane. Similar to that in the simultaneous adsorption mode, the difference between the HMSMD and MSMD models is narrowed with a decrease in propane concentration in the displacement dynamics of ethane by propane.

The displacement kinetics of propane by ethane in Ajax carbon of 1/16 in. diameter cylinders with different concentration combinations are shown in Figure 13. The HMSMD

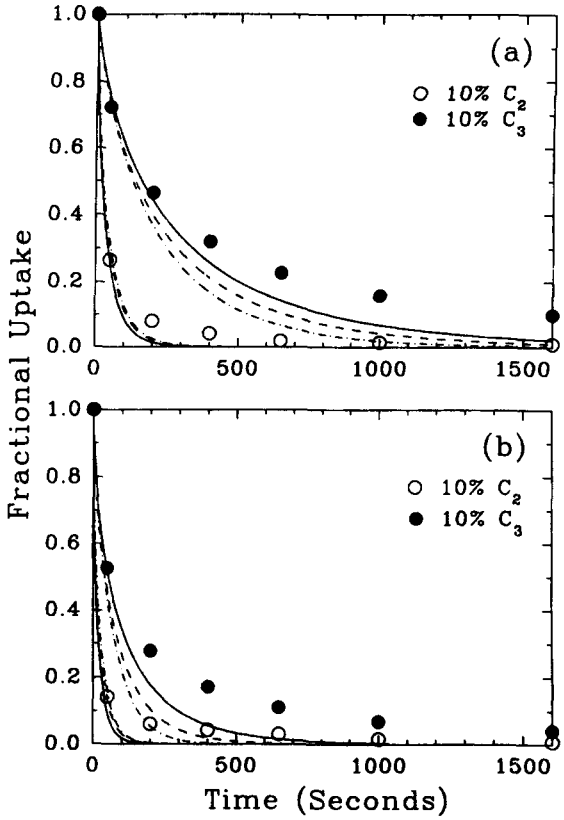

Figure 10. Binary desorption dynamics of 10% ethane and 10% propane in Ajax activated carbon at 60°C, 1 atm.

(a) 2.6 mm slab; (b) 1/16 in. (1.6 mm) cylinder. (——) HMSMD; (- - - -) MSMD; (-•-•-•-) CMSMD.

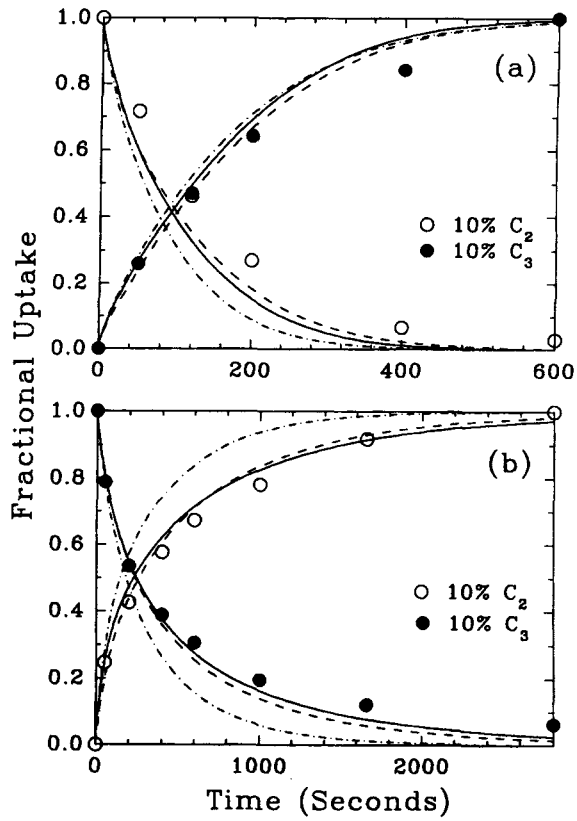

Figure 11. Displacement dynamics of ethane and propane in Ajax activated carbon of 2.6 mm slabs at 30°C, 1 atm.

(——) HMSMD; (- - - -) MSMD; (-•-•-•-) CMSMD.

model best describes the experimental data, followed by the MSMD model. The agreement between the CMSMD model and the data is very poor, because the desorbed species is propane. This is consistent with the studies of single-component systems where the desorption dynamics of propane is mostly affected by the choice of models (Hu et al., 1993). The difference between the displacement and single-component systems is that three model predictions also significantly differ in the adsorption rate of ethane due to the interactions in the displacement mode, although the single-component adsorption kinetic data of ethane is fitted well by all three models. The effect of energy distribution is more important with a lower ethane concentration (see HMSMD and MSMD in Figure 13) which is also true for simultaneous adsorption.

The displacement dynamics of ethane and propane in Ajax activated carbon at other temperatures, 10 and 60°C, are shown in Figures 14 and 15, respectively. Again the CMSMD model is found to poorly predict the experimental data in the case of *propane displaced by ethane*. The effects of concentration dependent surface diffusion and energy distribution become less important when temperature increases, as expected.

Conclusions

By using information of single-component equilibrium and mass transfer, the MSMD and HMSMD models are found to be able to predict the multicomponent adsorption dynamics. In all studies of binary adsorption of ethane and propane onto 4.4 mm slabs and 1/16 in. (1.6 mm) cylinders of Ajax activated carbon at various concentrations of ethane and propane and different temperatures, the HMSMD and MSMD model predictions describe the experimental data well. In particular these two models accurately predict the degree of overshoot of the faster-diffusing/less strongly-adsorbed species. On the other hand, the CMSMD model proposed by Do and coworkers (Gray and Do, 1990; Mayfield and Do, 1991) fails to predict the multicomponent adsorption kinetics using parameters extracted from single-component systems. The agreement between the CMSMD model and the experimental data is generally poor. Therefore, it is necessary to consider the concentration dependent surface diffusion in the mathematical modeling. The effect of surface energetic heterogeneity is more pronounced at lower temperatures, lower ethane concentrations and higher propane concentrations.

The contribution of concentration dependent surface diffusion on the simultaneous desorption dynamics of ethane and propane in Ajax activated carbon is found significant. The desorption rate of propane is seriously influenced by this effect, while that of ethane is less affected. The concentration dependent surface diffusion becomes more important at a lower temperature. This is also true for the effect of energy distribution on binary desorption. Therefore, the HMSMD model

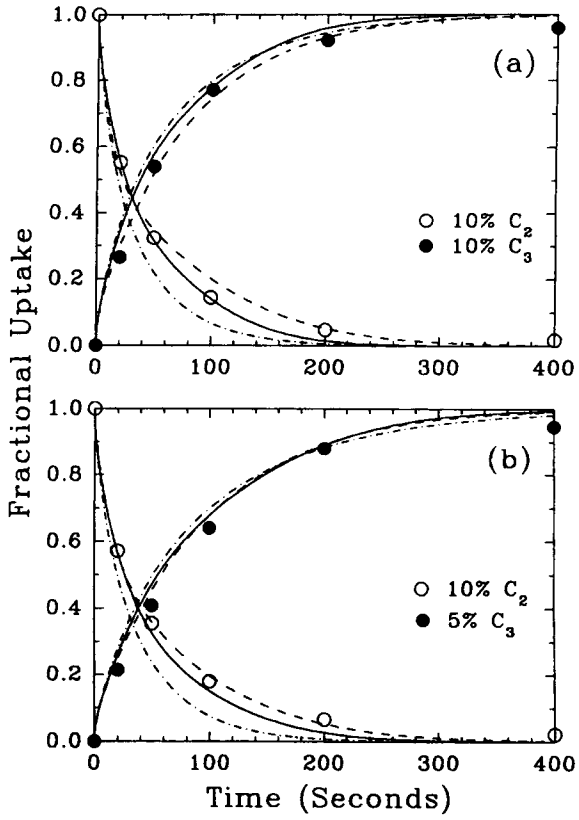

Figure 12. Dynamics of ethane displaced by propane in Ajax activated carbon of 1/16 in. (1.6 mm) diameter cylinders at 30°C, 1 atm.

(——) HMSMD; (- - - -) MSMD; (-•-•-•-) CMSMD.

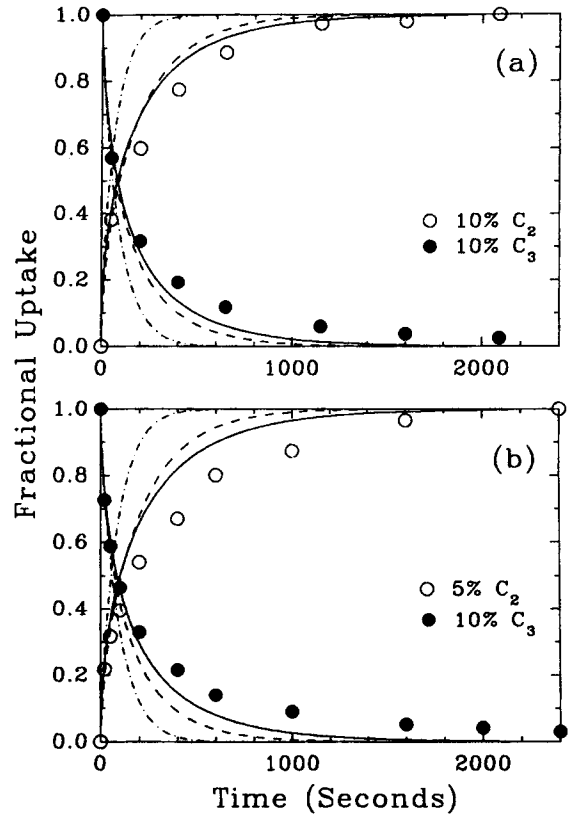

Figure 13. Dynamics of propane displaced by ethane in Ajax activated carbon of 1/16 in. (1.6 mm) diameter cylinders at 30°C, 1 atm.

(——) HMSMD; (- - - -) MSMD; (-•-•-•-) CMSMD.

is recommended in the modeling of simultaneous desorption dynamics.

The effect of energy distribution on the displacement kinetics of Ajax carbon is usually not important when ethane is displaced by propane. The HMSMD model provides better predictions over the MSMD model only in the case of *propane displaced by ethane* where the desorbed species is propane. The CMSMD model, on the other hand, is in serious error with the experimental data when *propane is displaced by ethane.*

In summary, the HMSMD model best describes the experimental data in all cases of binary adsorption, desorption and displacement kinetics of ethane and propane in Ajax activated carbon. The MSMD model using the IAS-Unilan equation is also in reasonably good agreement with the experimental data in simultaneous adsorption and displacement modes. The CMSMD model, on the other hand, is strongly discouraged in the studies of multicomponent sorption kinetics due to its very poor performance in the predictions of the multicomponent data.

Acknowledgment

This project is supported by the Australian Research Council and the REGS of the University of Queensland.

Notation

a = ratio of the surface activation energy to the heat of adsorption
b = isotherm parameter (m^3/kmol)
b_0 = isotherm parameter (m^3/kmol)
Bi = Biot number (defined in Table 1)
CMSMD = constant surface diffusivity macropore, surface and micropore diffusion
C_b = adsorbate concentration in the bulk (kmol/m^3)
C_{im} = imaginary adsorbate concentration inside the microparticle (kmol/m^3)
C_p = adsorbate concentration in the macropore (kmol/m^3)
C_{pi} = initial adsorbate concentration in the macropore (kmol/m^3)
C_0 = characteristic concentration for the fluid concentration (kmol/m^3)
C_μ = adsorbed concentration in the particle (kmol/m^3)
$C_{\mu 0}$ = characteristic concentration for the adsorbed concentration (kmol/m^3)
$C_{\mu,obs}$ = observed adsorbed concentration in the particle (kmol/m^3)
$C_{\mu s}$ = maximum adsorption capacity (kmol/m^3)
D_p = macropore diffusivity (m^2/s)
D_μ = surface diffusivity (m^2/s)
$D_{\mu 0}$ = surface diffusivity at zero energy level (m^2/s)
e = nondimensional energy (defined in Table 1)
E = adsorbate-adsorbent interaction energy (kJ/mol)
f = nondimensional energy distribution function (defined in Table 1)
F = energy distribution function
GC = gas chromatography
H = function defined in Table 1
HMSD = heterogeneous macropore and surface diffusion
HMSMD = heterogeneous macropore, surface and micropore diffusion
IAS = ideal adsorbed solution
J_p = flux through the macropore (kmol/(m^2·s))
J_μ = flux through the solid (kmol/(m^2·s))

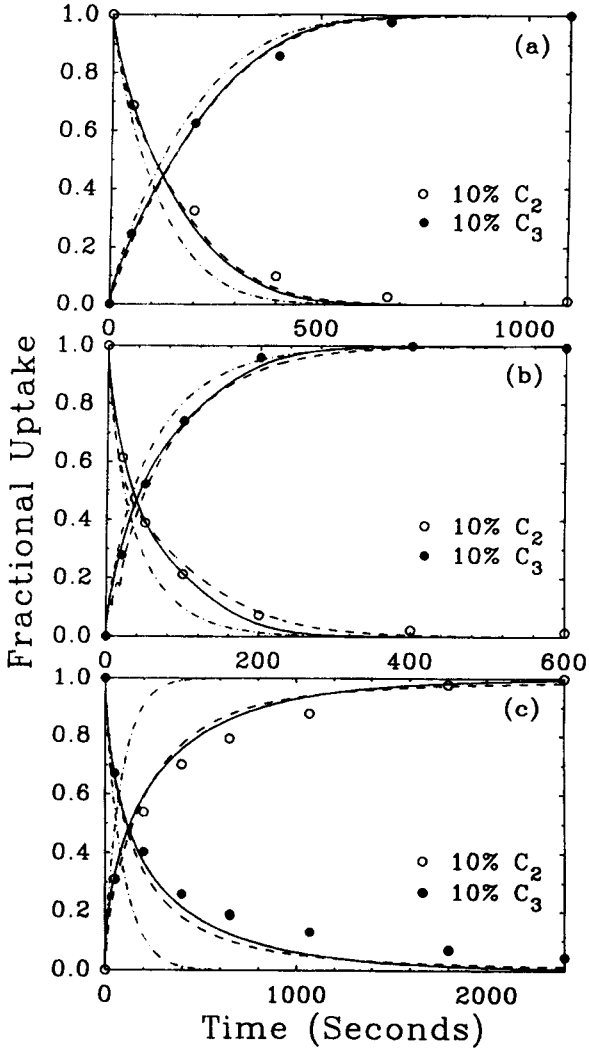

Figure 14. Displacement dynamics of ethane and propane in Ajax activated carbon at 10°C, 1 atm.

(a) 2.6 mm slab; (b), (c) 1/16 in. (1.6 mm) cylinder. (——) HMSMD; (- - - -) MSMD; (-•-•-•-) CMSMD.

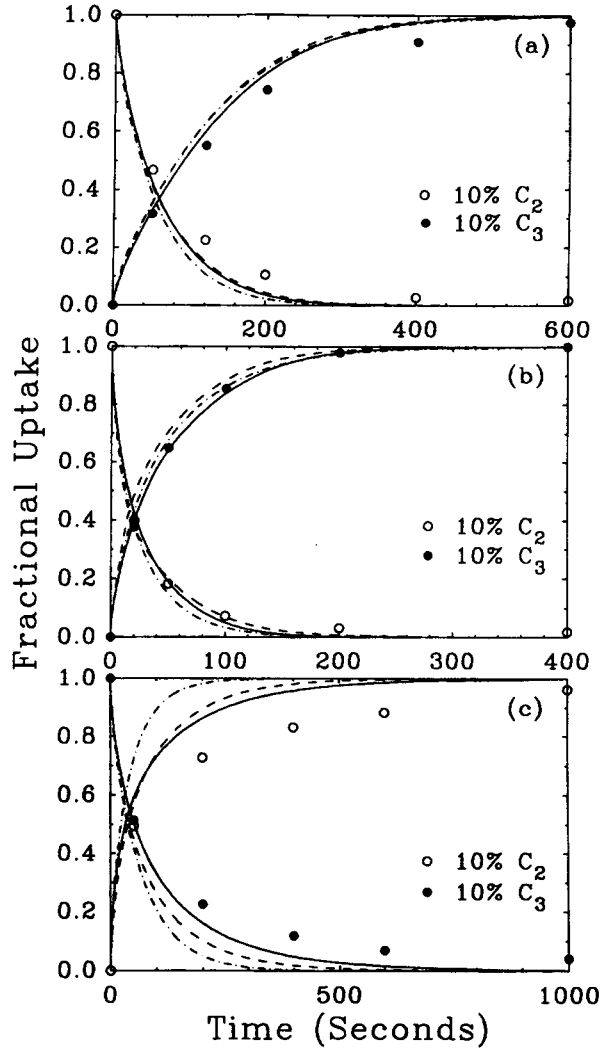

Figure 15. Displacement dynamics of ethane and propane in Ajax activated carbon at 60°C, 1 atm.

(a) 2.6 mm slab; (b), (c) 1/16 in. (1.6 mm) cylinder. (——) HMSMD; (- - - -) MSMD; (-•-•-•-) CMSMD.

k_m = film mass-transfer coefficient (m/s)
MSMD = macropore, surface and micropore diffusion
NC = number of component
r = particle radial position (m)
r_μ = microparticle radial position (m)
R = particle radius (m)
R_g = gas constant (kJ/(kmol·K))
R_μ = diffusion length of the microparticle (m)
s = geometric factor (=0, 1, 2 for slab, cylinder and sphere, respectively)
s_μ = geometric factor of the microparticle
t = time (s)
T = temperature (K)
we = Gaussian quadrature weight
x = nondimensional particle coordinate
x_μ = nondimensional microparticle coordinate
Y = nondimensional adsorbate concentration in the macropore
Y_b = nondimensional adsorbate concentration in the bulk
Y_{im} = nondimensional imaginary adsorbate concentration inside the microparticle
Y_μ = nondimensional adsorbed concentration in the particle

Greek letters

β^2 = ratio of the zero coverage surface diffusivity in the microparticle coordinate to that in the particle coordinate
γ = nondimensional model parameter defined in Table 1
δ = nondimensional model parameter defined in Table 1
ϵ_M = particle macropore porosity
η = nondimensional model parameter defined in Table 1
λ = nondimensional model parameter defined in Table 1
σ = nondimensional model parameter defined in Table 1
σ_μ = nondimensional model parameter defined in Table 1
τ = nondimensional time defined in Table 1

Literature Cited

Do, D. D., and X. Hu, "An Energy Distributed Model for Adsorption Kinetics in Large Heterogeneous Microporous Particles," *Chem. Eng. Sci.*, **48**, 2119 (1993).

Gray, P. G., and D. D. Do, "Adsorption and Desorption of Gaseous Sorbates on a Bidispersed Particle with Freundlich Isotherm. III. Contribution of Surface Diffusion to the Sorption Dynamics of Sulphur Dioxide on Activated Carbon," *Gas Separation and Purification*, **4**, 149 (1990).

Horas, J. A., H. A. Saitua, and J. Marchese, "Surface Diffusion of Adsorbed Gases on an Energetically Heterogeneous Porous Solid," *J. Colloid Interface Sci.*, **126**, 421 (1988).

Hu, X., "Fundamental Studies of Multicomponent Adsorption, Desorption and Displacement Kinetics of Light Hydrocarbons in Activated Carbon," PhD Thesis, University of Queensland, Australia (1992).

Hu, X., and D. D. Do, "Effect of Surface Energetic Heterogeneity on the Kinetics of Adsorption of Gases in Microporous Activated Carbon," *Langmuir* (in press, 1993a).

Hu, X., and D. D. Do, "Multicomponent Adsorption Kinetics of Hydrocarbons onto Activated Carbon: Contribution of Micropore Resistance," *Chem. Eng. Sci.* (in press, 1993b).

Hu, X., G. N. Rao, and D. D. Do, "Effect of Energy Distribution on Sorption Kinetics in Bidispersed Particles," *AIChE J.*, **39**(2), 249 (1993).

Kapoor, A., and R. T. Yang, "Surface Diffusion on Energetically Heterogeneous Surfaces," *AIChE J.*, **35**, 1735 (1989).

Kapoor, A., and R. T. Yang, "Surface Diffusion on Energetically Heterogeneous Surfaces—An Effective Medium Approximation Approach," *Chem. Eng. Sci.*, **45**, 3261 (1990).

Kapoor, A., J. A. Ritter, and R. T. Yang, "An Extended Langmuir Model for Adsorption of Gas Mixtures on Heterogeneous Surfaces," *Langmuir*, **6**, 660 (1990).

Mayfield, P. L. J., and D. D. Do, "Measurement of the Single-Component Adsorption Kinetics of Ethane, Butane and Pentane onto Activated Carbon Using a Differential Adsorption Bed," *Ind. Eng. Chem. Res.*, **30**, 1262 (1991).

Misra, D. N., "New Adsorption Isotherm for Heterogeneous Surfaces," *J. Chem. Phys.*, **52**, 5499 (1970).

Moon, H., and C. Tien, "Adsorption of Gas Mixtures on Adsorbents with Heterogeneous Surfaces," *Chem. Eng. Sci.*, **41**, 2967 (1988).

Myers, A. L., "Adsorption of Pure Gases and Their Mixtures on Heterogeneous Surfaces," in *Fundamentals of Adsorption*, A. L. Myers and G. Belfort, eds., Engineering Foundation, New York, pp. 365-381 (1984).

Okazaki, M., H. Tamon, and R. Toei, "Interpretation of Surface Flow Phenomenon of Adsorbed Gases by Hopping Model," *AIChE J.*, **27**, 262 (1981).

Petzold, L. R., "A Description of DASSL: A Differential/Algebraic Equation System Solver," *Sandia Technical Report: SAND 82-8637*, Livermore, CA (1982).

Roginski, S. S., *Adsorption and Catalysis on Heterogeneous Surfaces*, Academy of Sciences of USSR, Moscow, in Russian (1948).

Roginski, S. S., *Adsorption und Katalyse an Homogenen Oberflachen*, Akademie, Berlin (1958).

Ross, S., and J. P. Olivier, "On Physical Adsorption. XII. The Adsorption Isotherm and the Adsorptive Energy Distribution of Solids," *J. Phys. Chem.*, **65**, 608 (1961).

Ruthven, D. M., *Principles of Adsorption and Adsorption Processes*, Wiley, New York (1984).

Seidel, A., and P. Carl, "The Concentration Dependence of Surface Diffusion for Adsorption on Energetically Heterogeneous Adsorbents," *Chem. Eng. Sci.*, **44**, 189 (1989).

Sircar, S., "New Adsorption Isotherm for Energetically Heterogeneous Adsorbents," *J. Colloid Interface Sci.*, **98**, 306 (1984).

Sircar, S., and A. L. Myers, "Equilibrium Adsorption of Gases and Liquids on Heterogeneous Adsorbents—A Practical Viewpoint," *Surface Sci.*, **205**, 353 (1988).

Valenzuela, D. P., A. L. Myers, O. Talu, and I. Zwiebel, "Adsorption of Gas Mixtures: Effect of Energetic Heterogeneity," *AIChE J.*, **34**, 397 (1988).

Villadsen, J., and M. L. Michelsen, *Solution of Partial Differential Equation Models by Polynomial Approximation*, Prentice-Hall, Englewood Cliffs, NJ (1978).

Zgrablich, G., V. Pereyra, M. Ponzi, and J. Marchese, "Connectivity Effects for Surface Diffusion of Adsorbed Gases," *AIChE J.*, **32**, 1158 (1986).

Manuscript received Dec. 18, 1992, and revision received Mar. 1, 1993.